Karlsruhe Institute of Technology

Wave phenomena
analysis and numerics

A localized orthogonal decomposition method for heterogeneous mixed-dimensional problems

Moritz Hauck, Axel Målqvist, Malin Mosquera

CRC Preprint 2025/47, October 2025

KARLSRUHE INSTITUTE OF TECHNOLOGY

CRC 1173

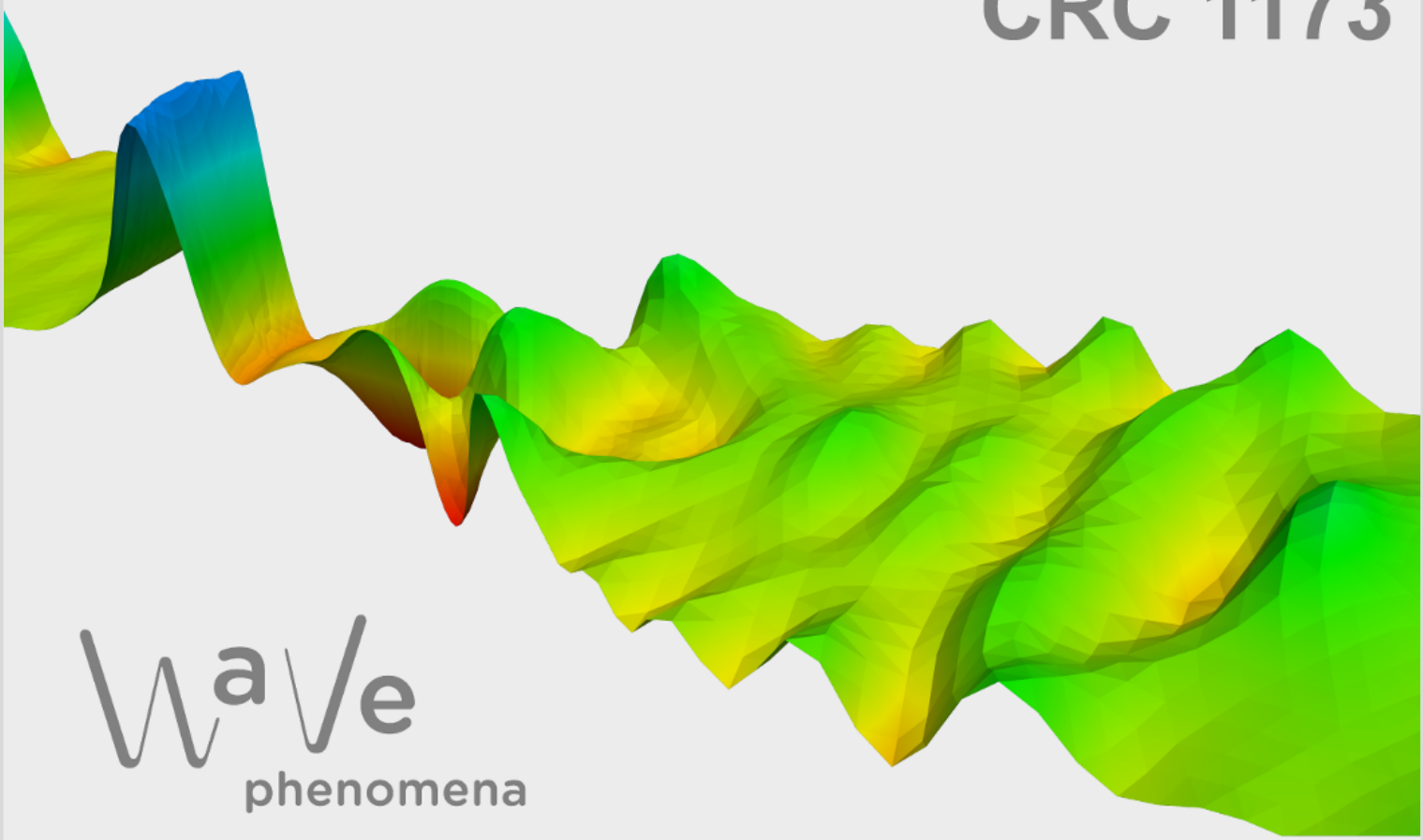

Wave phenomena

Participating universities

UNIVERSITÄT BONN

Universität Stuttgart

EBERHARD KARLS UNIVERSITÄT TÜBINGEN

TU WIEN

Funded by

DFG

ISSN 2365-662X

A LOCALIZED ORTHOGONAL DECOMPOSITION METHOD FOR HETEROGENEOUS MIXED-DIMENSIONAL PROBLEMS

MORITZ HAUCK*, AXEL MÅLQVIST†, MALIN MOSQUERA†

Abstract. We propose a multiscale method for mixed-dimensional elliptic problems with highly heterogeneous coefficients arising, for example, in the modeling of fractured porous media. The method is based on the Localized Orthogonal Decomposition (LOD) framework and constructs locally supported, problem-adapted basis functions on a coarse mesh that does not need to resolve the coefficient oscillations. These basis functions are obtained in parallel by solving localized fine-scale problems. Our a priori error analysis shows that the method achieves optimal convergence with respect to the coarse mesh size, independent of the coefficient regularity, with an exponentially decaying localization error. Numerical experiments validate these theoretical findings and demonstrate the computational viability of the method.

1. Introduction

The simulation of physical processes in highly heterogeneous media is challenging, especially when the material contains thin structures such as fractures, cracks, or reinforcements. Resolving these features explicitly in large scale simulation can be prohibitively expensive, potentially exceeding the available computing resources. A common and effective alternative is to model these thin structures as lower-dimensional interfaces, embedded within a higher-dimensional bulk domain. Such problems arise in many applications, most prominently in the modeling of flow through fractured porous media. In this context, the fractures are modeled as lower-dimensional manifolds with effective interface conditions; see, e.g., [MJR05, AGPR19, BNY18, DPFS17, FK18]. Related problems include modeling vascular networks embedded in biological tissue; see [FKO+22].

From a numerical perspective, solving mixed-dimensional PDEs presents several challenges. Classical finite element methods require meshes that resolve the complex geometry of embedded features, which can become intractable for a large number of interfaces. The situation is further complicated by the presence of strongly heterogeneous and oscillatory coefficients, which must also be resolved by the considered meshes. This situation is typical in porous media flow where the permeability varies rapidly in the bulk regions between interfaces. This paper focuses precisely on such a setting: we study a mixed-dimensional, elliptic diffusion problem with highly heterogeneous coefficients.

Many numerical methods have been developed for solving partial differential equations on surfaces. A foundational contribution to the finite element approximation of the Laplace–Beltrami equation was given in [Dzi88], where the method is formulated on a polyhedral approximation of the surface (see also the comprehensive overview in [DE13]). Alternative approaches include trace-based methods [BHL+18, BCH+14, ORG09], in which surface functions are represented as traces of functions defined in a higher-dimensional ambient space. Finite element

2020 *Mathematics Subject Classification.* 65N12, 65N15, 65N30.

Key words and phrases. mixed-dimensional PDEs, rough coefficients, multiscale method, a priori error analysis, exponential decay.

methods for coupled bulk–interface problems have also been the subject of extensive research; see, for example, [ER12, MJR05]. More recently, a fitted finite element method has been introduced in [HMM23b], with particular emphasis on establishing Poincaré-type inequalities for the coupled bulk–interface model.

To address the challenges posed by heterogeneous coefficients in elliptic model problems, a wide range of multiscale methods have been developed. These methods aim to construct low-dimensional problem-adapted approximation spaces that effectively capture fine-scale features. The corresponding basis functions are typically associated with mesh entities of a coarse mesh and computed by solving local fine-scale problems. Prominent approaches include the Heterogeneous Multiscale Method (HMM)[EE03, EE05], (Generalized) Multiscale Finite Element Methods (GMsFEM) [BO83, BCO94], Multiscale Spectral Generalized Finite Element Methods [BL11, MSD22], the Localized Orthogonal Decomposition (LOD) method [MP14, HP13], and gamblets [Owh17, OS19]. More recently, refined localization strategies within the LOD framework have been proposed; see, e.g., [HP23, FHKP24]. For a comprehensive survey of these methods, we refer to [AHP21]. In [HMW21], an initial step toward extending the LOD method to mixed-dimensional models was taken. However, that approach enforces the continuity of the solution across interfaces, making it more restrictive than the setting considered here. Moreover, the methods differ fundamentally: our construction is explicitly tailored to domains with a fractured structure. This allows us to relax the geometric assumptions on the interface and to improve the localization properties of the method.

This paper proposes a multiscale method, in the spirit of the LOD method, for the mixed-dimensional model problem with heterogeneous coefficients. Similar to the classical elliptic setting, the method decomposes the underlying energy space into an infinite-dimensional fine-scale space characterized by the vanishing of integrals with respect to coarse mesh entities, and a finite-dimensional complement space. Crucially, the complement space is defined with respect to the energy inner product, thereby adapting it to the multiscale problem at hand. The canonical basis functions of the complement space are associated with coarse mesh entities and exhibit exponential decay with respect to the coarse mesh. This motivates their localization to patches of elements of the coarse mesh. The precise way the localized basis functions are defined is inspired by the recent work [HLM25] in the classical elliptic setting. We provide a rigorous a priori error analysis of the proposed method in the mixed-dimensional setting, showing that the error consists of two terms. The first term is an optimal-order term in the coarse mesh size. The second term decays exponentially with the number of element layers of the patches used for localization. Thus, increasing the number of element layers logarithmically with the desired accuracy yields an optimally convergent approximation. Numerical experiments are included to validate and support the theoretical results.

The remainder of the paper is organized as follows. In Section 2, we introduce the mixed-dimensional model problem. A prototypical multiscale method that achieves optimal convergence rates under minimal structural assumptions is presented in Section 3. In Section 4, we establish the exponential decay of the corresponding prototypical basis functions, motivating their localization, which is discussed in Section 5. Based on the resulting localized basis functions, a practical multiscale method is developed in Section 6. In Section 7 we extend the methodology to allow for interfaces that vary of the fine computational mesh. Finally, in Section 8, we present a series of numerical experiments that support our theoretical findings.

2. Mixed-dimensional model problem

This section introduces the mixed-dimensional model problem considered in this paper. We begin by specifying the underlying mixed-dimensional geometry.

2.1. **Geometry.** Consider a Lipschitz domain $\Omega \subset \mathbb{R}^d$, $d \in \{2, 3\}$, partitioned into $d+1$ not necessarily connected subdomains of varying dimensionalities as follows:

$$\Omega = \Omega^0 \cup \cdots \cup \Omega^d, \tag{2.1}$$

where c in Ω^c denotes the codimension ($0 \leq c \leq d$). Each Ω^c is decomposed into finitely many disjoint and connected subdomain segments indexed by a set L_c, as

$$\Omega^c = \bigcup_{\ell \in L_c} \Omega^c_\ell, \tag{2.2}$$

where each Ω^c_ℓ is contained in a planar hypersurface of codimension c.

To formulate assumptions on the topology of the problem, we define, for each codimension c, a topological subspace $X^c \subset \mathbb{R}^d$. For codimension $c = 0$, we set $X^0 = \Omega$, and for codimensions $c > 0$, we define $X^c = X^{c-1} \setminus \Omega^{c-1}$. Standard topological concepts such as openness, closedness, and density are understood with respect to the subspace topology on X^c. The closure, boundary, and interior operators are denoted by $\bar{\cdot}$, $\partial\cdot$, and $\mathrm{int}(\cdot)$, respectively. We assume that each subdomain segment Ω^c_ℓ, for $\ell \in L_c$, is open in X^c, and that their union Ω^c is dense in X^c. Furthermore, we suppose that for any pair $(i, j) \in L_c \times L_{c+1}$, we either have the inclusion $\Omega^{c+1}_j \subseteq \partial\Omega^c_i$ or it holds $\Omega^{c+1}_j \cap \overline{\Omega^c_i} = \emptyset$. This condition allows us to define an adjacency relation E^c between segments of codimensions c and $c+1$ as

$$(i, j) \in E^c \quad \text{if} \quad \Omega^{c+1}_j \subseteq \partial\Omega^c_i, \tag{2.3}$$

and to represent boundary integrals over subdomain segments as sums of subdomain segments of one higher codimension. In what follows, we focus on subdomains of codimensions 0, 1, and 2. To simplify the considered setting, we assume that all subsets Ω^c_ℓ have Lipschitz boundaries and are polyhedra, polygons, line segments, or points, according to their dimension. This assumption excludes pathological cases such as slit domains and ensures, for example, that an interface cannot end within a bulk region without connecting to another interface. For an example of a domain satisfying these requirements, see Figure 2.1.

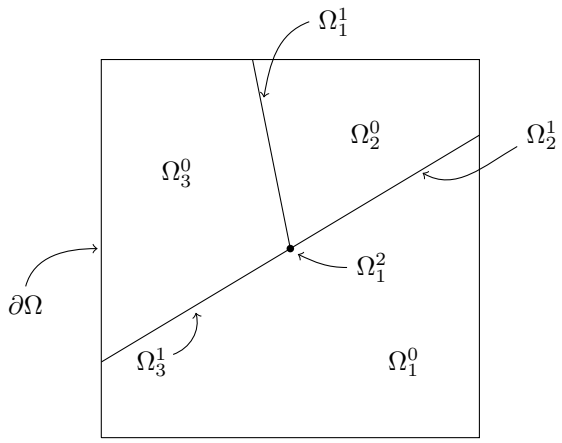

Figure 2.1. An example satisfying our assumptions for $d = 2$, with subdomain segments of codimensions $c = 0, 1, 2$ indicated.

2.2. **Function spaces.** For a measurable set $\omega \subset \mathbb{R}^d$, we denote by $L^2(\omega)$ the Lebesgue space of square-integrable functions on ω, and by $H^1(\omega)$ the Sobolev space consisting of functions in $L^2(\omega)$ whose weak derivatives also belong to $L^2(\omega)$. The $L^2(\omega)$-inner product is denoted by $(\cdot,\cdot)_\omega$, with induced norm $\|\cdot\|_{L^2(\omega)}$. The $H^1(\omega)$-norm is denoted by $\|\cdot\|_{H^1(\omega)}$. In the case that the subdomain ω is a subdomain segment of codimension $c > 0$, we interpret $H^1(\omega)$ as $H^1(\widehat{\omega})$, where $\widehat{\omega} \subset \mathbb{R}^{d-c}$ is the image of ω under a rigid coordinate transformation. This allows to use of standard tools such as differential operators, the Poincaré inequality, Green's theorem, and trace theorems on $\mathbb{R}^{d-c}$. For clarity, we denote the gradient on subdomain segments of codimension c by ∇^c with the convention $\nabla = \nabla^0$.

We introduce the product space

$$V := V^0 \times V^1,$$

where the space V^0, defined on the bulk domain of codimension 0, is broken along the interfaces between subdomain segments. Specifically,

$$V^0 := \prod_{i \in L^0} H^1(\Omega_i^0),$$

recalling that Ω^0 is the disjoint union of the subdomains $\{\Omega_i^0\}_{i \in L^0}$. The space V^1 is defined on the interfaces of codimension 1. Continuity is enforced across shared boundaries, which are formed by subdomain segments of codimension 2, so that

$$V^1 := \Big\{ v \in \prod_{j \in L^1} H^1(\Omega_j^1) \,:\, v_j|_{\Omega_k^2} = v_{j'}|_{\Omega_k^2} \text{ for all } (j,k),(j',k) \in E^1 \Big\},$$

where the restriction of a function to a subdomain segment is indicated with a subscript index for the respective subdomain.

The subspaces of V^c for $c \in \{0,1\}$, which satisfy homogeneous Dirichlet boundary conditions on $\partial\Omega$ are defined as

$$V_0^c := \{ v^c \in V^c \,:\, v^c|_{\partial\Omega} = 0 \},$$

and their product space is denoted by

$$V_0 := V_0^0 \times V_0^1.$$

In the following, for a function $v \in V$, we write $v = (v^0, v^1)$ and equip the space V, and naturally the subspace V_0, with the product norm

$$\|v\|_V^2 := \|v^0\|_{H^1(\Omega^0)}^2 + \|v^1\|_{H^1(\Omega^1)}^2. \tag{2.4}$$

2.3. **Problem formulation.** The mixed-dimensional model problem involves coefficients defined on both the bulk domain and the interface domain. On the bulk domain Ω^0, we consider a coefficient $A^0 \in L^\infty(\Omega^0)$. Similarly, on the interface domain Ω^1, we introduce coefficients $A^1 \in L^\infty(\Omega^1)$ and $B^1 \in L^\infty(\Omega^1)$. These coefficients are assumed to satisfy uniform ellipticity and boundedness conditions: there exist positive constants $0 < \underline{\alpha} \le \overline{\alpha} < \infty$ and $0 < \underline{\beta} \le \overline{\beta} < \infty$ such that

$$\begin{aligned} \underline{\alpha} \le A^0(x) \le \overline{\alpha} \quad &\text{a.e. in } \Omega^0, \\ \underline{\alpha} \le A^1(x) \le \overline{\alpha}, \quad \underline{\beta} \le B^1(x) \le \overline{\beta} \quad &\text{a.e. in } \Omega^1. \end{aligned} \tag{2.5}$$

The bilinear form a of the mixed-dimensional model problem is then defined as

$$\begin{aligned} a(v,w) := {} & (A^0\nabla^0 v^0, \nabla^0 w^0)_{\Omega^0} + (A^1\nabla^1 v^1, \nabla^1 w^1)_{\Omega^1} \\ & + \sum_{(i,j)\in E^0} (B^1(v_i^0 - v_j^1), w_i^0 - w_j^1)_{\Omega_j^1}. \end{aligned} \tag{2.6}$$

Given a right-hand side functional

$$F(w) := (f^0, w^0)_{\Omega^0} + (f^1, w^1)_{\Omega^1}, \tag{2.7}$$

with source terms $f^0 \in L^2(\Omega^0)$, $f^1 \in L^2(\Omega^1)$, the mixed-dimensional model problem is formulated as follows: find $u \in V_0$ such that

$$a(u,v) = F(v), \quad \text{for all } v \in V_0. \tag{2.8}$$

The bulk and interface domains are coupled through a Robin-type boundary condition. Continuity of the solution across interface segments is enforced, and a Kirchhoff-type law governs the flux exchange between adjacent interface segments.

If the solution and data are sufficiently smooth, the weak formulation in (2.8) is equivalent to the strong formulation of finding $u \in V_0$ such that

$$\begin{aligned} -\nabla \cdot \big(A^0 \nabla u^0\big) &= f^0, && \text{in } \Omega^0, \\ -\nabla^1 \cdot \big(A^1 \nabla^1 u^1\big) - \sum_{(i,j)\in E_0} B^1\big(u_i^0 - u_j^1\big) &= f^1, && \text{in } \Omega^1, \end{aligned}$$

subject to homogeneous Dirichlet conditions on the exterior boundary, continuity of both solution and flux at interface junctions, and the following Robin-type coupling between bulk and interface domains:

$$n_{\Omega_i^0} \cdot \big(A^0 \nabla u_i^0\big) + B^1 u_i^0 = B^1 u_j^1, \qquad \text{on } \partial\Omega_i^0 \cap \Omega_j^1$$

for all i, j such that the intersection is non-trivial. Here, n_ω denotes the outward unit normal of the subdomain ω. The solution of this equation can for example model the pressure in a heterogeneous medium in the presence of cracks or faults. Further details can be found in [HMM23b].

We close this section by establishing coercivity and boundedness of the bilinear form a, which, since V_0 is a Hilbert space when equipped with the norm (2.4), ensures the well-posedness of problem (2.8) by the Riesz representation theorem.

Lemma 2.1 (Properties of a)**.** *There exist constants $0 < c_a \le C_a < \infty$, such that*

$$a(v,v) \ge c_a \|v\|_V^2, \quad v \in V_0, \qquad a(v,w) \le C_a \|v\|_V \|w\|_V, \quad v, w \in V_0,$$

where, up to constants solely dependent on the geometry of $\{\Omega_\ell^c\}_{c,\ell}$, the constants scale as $c_a \sim (\underline{\alpha}^{-1} + \underline{\beta}^{-1})^{-1}$ and $C_a \sim (\overline{\alpha} + \overline{\beta})$.

A direct consequence of this result is that $\|\cdot\|_a^2 \coloneqq a(\cdot,\cdot)$ defines a norm on V_0, which will henceforth be referred to as the energy norm.

Proof. The coercivity proof employs an iterative procedure, starting by bounding norms on subdomain segments far from the domain boundary and progressively extending these bounds to neighboring segments until reaching those where a Friedrichs-type inequality applies; see [HMM23b, Lem. 1] for details. The boundedness can be proved using a standard trace inequality; see [HMM23b, Lem. 2]. □

3. Prototypical method

This section presents a prototypical multiscale method that achieves optimal-order approximations without any pre-asymptotic effects, under minimal structural assumptions on the coefficients. The LOD method is typically defined with respect to a coarse mesh of the domain. In the present mixed-dimensional setting, coarse meshes are required for both the bulk domain and the interface domain, denoted by $\mathcal{T}_H^0$ and $\mathcal{T}_H^1$, respectively. They are henceforth referred to as the *bulk mesh* and the *interface mesh*, respectively. Note that the considered coarse meshes are not required to resolve the fine-scale variations of the coefficients. In general, there is considerable flexibility in how these meshes are chosen. Even complex-shaped elements representing fractures can be accommodated, provided the elements are non-degenerate and a local element-wise Poincaré inequality holds.

Subsequently, we restrict our attention to a significantly simplified setting; see Section 7 for an extension of the methodology to more general meshes. Specifically, we consider a bulk mesh that is a quasi-uniform partition of Ω into finitely many closed, shape-regular simplicial or quadrilateral/hexahedral elements, with diameter at most $H > 0$. We assume that the bulk mesh is such that each bulk subdomain segment Ω_i^0 can be expressed as a union of bulk mesh elements. Similarly, the interface mesh is assumed to be such that each interface subdomain segment Ω_j^1 can be expressed as a union of interface mesh elements. Moreover, we assume the compatibility condition that any face of a bulk mesh element lying on an interface Ω_j^1 coincides exactly with an element of the interface mesh. Consequently, the mesh size H is also the maximal element diameter of the interface mesh.

Following the presentation of the LOD in [AHP21], the definition of the method is based on so-called *quantities of interest* (QOI). Their purpose is to encode which information about the solution u to problem (2.8) the prototypical multiscale method should preserve exactly. Each QOI is associated with an element of either the bulk or the interface mesh and is defined as the corresponding element-wise average:

$$q_{T^c}(v) := \frac{1}{|T^c|_{d-c}} \int_{T^c} v^c \,\mathrm{d}x, \quad T^c \in \mathcal{T}_H^c,\ c \in \{0,1\}, \tag{3.1}$$

where $|\cdot|_n$ for $n \in \{d-1, d\}$ denotes the n-dimensional volume. Based on these QOI, we can now define a so-called *fine-scale space* as

$$W := \{v \in V_0 \,:\, q_{T^c}(v) = 0 \text{ for all } T^c \in \mathcal{T}_H^c,\ c \in \{0,1\}\}\,. \tag{3.2}$$

Intuitively, this space consists of functions that average out on length scales smaller than or equal to H. It represents the fine-scale information that cannot be captured on the coarse scale.

The approximation space of the prototypical multiscale method is then defined as the (finite-dimensional) orthogonal complement of the fine-scale space W in V_0, with respect to the energy inner product a, i.e.,

$$\tilde{V}_H := \{v \in V_0 \,:\, a(v,w) = 0 \text{ for all } w \in W\}\,. \tag{3.3}$$

Since $\tilde{V}_H$ is constructed as the orthogonal complement of W with respect to a, it inherently encodes problem-specific information. This enables reliable approximations even at scales where the coefficients are not resolved. The use of tildes in the notation serves to emphasize that the space is adapted to the problem at hand. A basis for the space $\tilde{V}_H$ can be constructed as outlined in the following lemma.

Lemma 3.1 (Prototypical basis)**.** *A basis of the space $\tilde{V}_H$ is given by*

$$\left\{\tilde{\varphi}_{T^c} \,:\, T^c \in \mathcal{T}_h^c,\, c \in \{0,1\}\right\} \tag{3.4}$$

with $\tilde{\varphi}_{T^c}$ defined for all $T^c \in \mathcal{T}_h^c$, $c \in \{0,1\}$ as the unique solutions to the saddle point problem: find $(\tilde{\varphi}_{T^c}, \lambda) \in V_0 \times \mathbb{R}^N$ with $N := \#\mathcal{T}_H^0 + \#\mathcal{T}_H^1$ such that

$$a(\tilde{\varphi}_{T^c}, v) \;+\; b(v,\lambda) \;=\; 0, \qquad \textit{for all } v \in V_0, \tag{3.5a}$$

$$b(\tilde{\varphi}_{T^c}, \mu) \;=\; \mu_{T^0}, \qquad \textit{for all } \mu \in \mathbb{R}^N, \tag{3.5b}$$

where the bilinear form $b\colon V \times \mathbb{R}^N \to \mathbb{R}$ is defined as

$$b(v,\mu) := \sum_{c\in\{0,1\}} \sum_{T^c \in \mathcal{T}_H^c} \mu_{T^c} q_{T^c}(v),$$

and μ_{T^c} denotes the component of the vector μ associated with the element T^c.

Before proving this lemma, we introduce the notion of bubble functions, which will be used not only in this proof but also throughout the manuscript. These are locally supported functions associated with either elements of the bulk or interface meshes and are denoted by b_{T^c} for $T^c \in \mathcal{T}_H^c$, $c \in \{0,1\}$. They are defined as

$b_{T^0} := (v_{T^0}, 0)$ for $T^0 \in \mathcal{T}_H^0$ and $b_{T^1} := (0, v_{T^1})$ for $T^1 \in \mathcal{T}_H^1$, where $v_{T^c} \in H_0^1(T^c)$ is chosen such that the resulting bubble function b_{T^c} satisfies the Kronecker-delta property:

$$q_{K^{c'}}(b_{T^c}) = \delta_{K^{c'}T^c}, \quad K^{c'} \in \mathcal{T}_H^{c'},\ c' \in \{0,1\}, \tag{3.6}$$

and such that the following stability estimate holds:

$$\|\nabla^c v_{T^c}\|_{L^2(T^c)} \lesssim H^{-1}\|v_{T^c}\|_{L^2(T^)} \lesssim H^{(d-c)/2-1}, \quad c \in \{0,1\}. \tag{3.7}$$

The construction of the functions v_{T^c} is classical; they can be obtained as suitably scaled products of hat functions. We emphasize that bubble functions only serve as a theoretical tool and are never used explicitly in practical implementations.

Proof of Lemma 3.1. We begin by establishing the well-posedness of problem (3.5) by verifying the inf–sup stability of the bilinear form b. Specifically, we show that there exists a constant $C > 0$ such that

$$\inf_{\mu \in \mathbb{R}^N} \sup_{v \in V} \frac{|b(v,\mu)|}{\|v\|_V\, |\mu|} \geq C, \tag{3.8}$$

where $|\cdot|$ denotes the Euclidean norm on $\mathbb{R}^N$.

Given any $\mu \in \mathbb{R}^N$, we construct a function $v \in V_0$ component-wise as

$$v := \sum_{c \in \{0,1\}} \sum_{T^c \in \mathcal{T}_H^c} \mu_{T^c}\, b_{T^c}$$

using the bubble functions introduced above. Noting that, by construction, we have $|b(v,\mu)| = |\mu|^2$, and employing the locality of the bubble functions together with a local Friedrichs inequality and the stability estimates from (3.7), we obtain

$$\|v\|_V^2 \lesssim \sum_{c \in \{0,1\}} \sum_{T^c \in \mathcal{T}_H^c} |\mu_{T^c}|^2 \|\nabla^c v_{T^c}\|_{L^2(T^c)}^2 \lesssim H^{d-2}|\mu|^2.$$

Combining these estimates establishes the inf–sup condition (3.8).

Next, we prove that (3.4) defines a basis for the space $\tilde{V}_H$. To this end, we first observe that condition (3.5a) implies that $\tilde{\varphi}_{T^c} \in \tilde{V}_H$ for all $T^c \in \mathcal{T}_H^c$, $c \in \{0,1\}$. To establish the basis property, let $v \in \tilde{V}_H$ be arbitrary, and define

$$w := v - \sum_{c \in \{0,1\}} \sum_{T^c \in \mathcal{T}_H^c} q_{T^c}(v)\tilde{\varphi}_{T^c}.$$

By construction, it holds that $w \in W$, and since w is also a-orthogonal to W, it follows that $w = 0$. Thus, any $v \in \tilde{V}_H$ can be expressed uniquely as a linear combination of functions in (3.4), which proves that they form a basis of $\tilde{V}_H$. This completes the proof. □

Having introduced the prototypical basis functions, we can define a projection operator $\mathcal{R}\colon V \to \tilde{V}_H$ which preserves the QOI from (3.1) by

$$\mathcal{R}v := \sum_{c \in \{0,1\}} \sum_{T^c \in \mathcal{T}_H^c} q_{T^c}(v)\tilde{\varphi}_{T^c}, \quad v \in V_0. \tag{3.9}$$

This operator coincides with the a-orthogonal projection onto $\tilde{V}_H$, since for any $v \in V_0$ and $w \in \tilde{V}_H$ it holds that $a(v - \mathcal{R}v, w) = 0$, noting that $v - \mathcal{R}v \in W$. This orthogonality relation also implies the continuity of $\mathcal{R}$, i.e.,

$$\|\mathcal{R}v\|_V \leq \sqrt{C_a/c_a}\|v\|_V, \quad v \in V_0, \tag{3.10}$$

where we have used Lemma 2.1.

The desired prototypical multiscale method then seeks $\tilde{u}_H \in \tilde{V}_H$ such that

$$a(\tilde{u}_H, \tilde{v}_H) = F(\tilde{v}_H) \quad \text{for all } \tilde{v}_H \in \tilde{V}_H, \tag{3.11}$$

where F is defined in (2.7). The following theorem proves optimal-order convergence of this method under minimal structural assumptions.

Theorem 3.2 (Prototypical method)**.** *The prototypical multiscale method* (3.11) *is well-posed, and its solution is given by* $\tilde{u}_H = \mathcal{R}u$*. Consider any right-hand side* F *of the form* (2.7) *with components satisfying* $f^0 \in H^s(\Omega^0)$ *and* $f^1 \in H^s(\Omega^1)$*, where* $s \in \{0, 1\}$*, and define a corresponding norm by*

$$|f|_s^2 := |f^0|_{H^s(\Omega^0)}^2 + |f^1|_{H^s(\Omega^1)}^2, \tag{3.12}$$

where $|\cdot|_{H^s}$ *denotes the* H^s*-seminorm. Then, the following error estimate holds:*

$$\|u - \tilde{u}_H\|_V \lesssim H^{1+s}|f|_s. \tag{3.13}$$

Proof. First, observe that the space $\tilde{V}_H$ is a closed subspace of V_0. Hence, by the Riesz representation theorem, problem (3.11) is well-posed. Comparing (3.3) with the weak formulation (2.8), we obtain that

$$a(u - \tilde{u}_H, \tilde{v}_H) = 0, \quad \tilde{v}_H \in \tilde{V}_H, \tag{3.14}$$

which shows that $\tilde{u}_H = \mathcal{R}u$ with the a-orthogonal projection $\mathcal{R}$ introduced above.

To derive the error estimate, we observe that $e := u - \tilde{u}_H$ lies in the space W. Using the coercivity result from Lemma 2.1, the orthogonality relation (3.14), and testing the weak formulation (2.8) with e, we obtain

$$c_a\|e\|_V^2 \leq a(e, e) = a(u, e) = F(e). \tag{3.15}$$

Let $\Pi_H^0 \colon L^2(\Omega^0) \to \mathbb{P}^0(\mathcal{T}_H^0)$ and $\Pi_H^1 \colon L^2(\Omega^1) \to \mathbb{P}^0(\mathcal{T}_H^1)$ denote the L^2-orthogonal projections onto piecewise constant functions on the coarse grid. Exploiting their orthogonality properties yields the following representation for $F(e)$:

$$F(e) = (f^0 - \Pi_H^0 f^0,\, e^0 - \Pi_H^0 e^0)_{\Omega^0} + (f^1 - \Pi_H^1 f^1,\, e^1 - \Pi_H^1 e^1)_{\Omega^1},$$

where the L^2-projections of f^0 and f^1 may be omitted without affecting the identity. Estimate (3.13) then follows by applying a local Poincaré-type inequality. □

4. Exponential decay of prototypical basis

We emphasize that the prototypical LOD basis functions defined in (3.4) are globally supported, and thus their computation requires solving global problems. However, this would be computationally infeasible in practice. In this section, we demonstrate that these basis functions exhibit an exponential decay, justifying their approximation by localized counterparts defined on oversampling domains, as will be discussed in Section 5. A practical multiscale method based on these localized basis functions will then be introduced in Section 6.

For the localization procedure, we adopt the approach proposed in the recent generalized framework for high-order LOD methods; see [HLM25]. This framework accommodates the choice of QOI on the bulk domain made here and enables a stable basis construction, ensuring that the error of the localized method does not increase as the coarse mesh is refined, when the oversampling parameter (the number of element layers composing the oversampling domains) remains fixed. Such negative effects have been observed, for example, in [MP14, Mai21]. Notably, this stability is achieved without relying on intricate bubble function constructions in the practical implementation of the method, cf. [HP22, DHM23]. The localization is based on a quasi-interpolation operator $\mathcal{I}_H \colon V \to V_H$, where $V_H := V_H^0 \times V_H^1$, with V_H^0 and V_H^1 denoting the conforming piecewise linear finite element spaces defined with respect to the bulk and interface meshes, respectively. In particular, we have $V_H \subset V$. The

operator is defined component-wise as $\mathcal{I}_H v = (\mathcal{I}_H^0 v, \mathcal{I}_H^1 v)$, where each component $\mathcal{I}_H^c v$ is defined at interior nodes z^c of the mesh $\mathcal{T}_H^c$ for codimension $c \in \{0,1\}$ as:

$$(\mathcal{I}_H^c v)(z^c) \coloneqq \frac{1}{\#\mathcal{T}^c(z^c)} \sum_{T^c \in \mathcal{T}^c(z^c)} q_{T^c}^c(v^c)\Lambda_{z^c}, \tag{4.1}$$

where $\mathcal{T}^c(z^c)$ denotes the set of elements in $\mathcal{T}_H^c$ sharing the node z^c, and Λ_{z^c} is the classical hat function associated with node z^c. For boundary nodes, the corresponding nodal values of $\mathcal{I}_H^c v$ are set to zero to conform to the prescribed Dirichlet boundary conditions. This operator satisfies for $c \in \{0,1\}$ the following local approximation and stability estimates:

$$\|v - \mathcal{I}_H^c v\|_{L^2(T^c)} + \|\nabla^c \mathcal{I}_H^c v\|_{L^2(T^c)} \lesssim \|\nabla^c v\|_{L^2(\mathsf{N}^c(T^c))}, \quad v \in V^c,\ T^c \in \mathcal{T}_H^c \tag{4.2}$$

with $\mathsf{N}^c(S^c)$ denoting the first-order element patch of a union of elements S^c in $\mathcal{T}_H^c$, defined as

$$\mathsf{N}^c(S^c) \coloneqq \bigcup \left\{ T^c \in \mathcal{T}_H^c \colon \overline{S^c} \cap \overline{T^c} \neq \emptyset \right\}. \tag{4.3}$$

Note that constructions such as (4.1) and the properties in (4.2) are classical; see, e.g., [EG17]. The specific choice of quasi-interpolation operator is not essential. Apart from the stability estimate (4.2), we only require that $\mathcal{I}_H v = 0$ holds for all $v \in W$.

Following the localization strategy in [HLM25], the a-orthogonal projection operator $\mathcal{R}$ defined in (3.9) is decomposed as:

$$\mathcal{R} = \mathcal{I}_H - \mathcal{K}, \tag{4.4}$$

where $\mathcal{K} \colon V_0 \to V_0$ maps any $v \in V_0$ to the unique solution $(\mathcal{K}v, \lambda) \in V_0 \times \mathbb{R}^N$ of

$$a(\mathcal{K}v, w) + b(w, \lambda) = a(\mathcal{I}_H v, w), \quad \text{for all } w \in V_0, \tag{4.5a}$$

$$b(\mathcal{K}v, \mu) = -\, b(v - \mathcal{I}_H v, \mu), \quad \text{for all } \mu \in \mathbb{R}^N. \tag{4.5b}$$

Note that λ is a generic notation for a Lagrange multiplier; the specific multiplier being referred to will be clear from the context.

The operator $\mathcal{K}$ can be decomposed as

$$\mathcal{K} = \sum_{T^0 \in \mathcal{T}_H^0} \mathcal{K}_{T^0},$$

where each local operator $\mathcal{K}_{T^0} \colon V_0 \to V_0$ maps any $v \in V_0$ to the unique solution $(\mathcal{K}_{T^0} v, \lambda) \in V_0 \times \mathbb{R}^N$ of

$$a(\mathcal{K}_{T^0} v, w) + b(w, \lambda) = a_{T^0}(\mathcal{I}_H v, w), \quad \text{for all } w \in V_0, \tag{4.6a}$$

$$b(\mathcal{K}_{T^0} v, \mu) = -\, b_{T^0}(v - \mathcal{I}_H v, \mu), \quad \text{for all } \mu \in \mathbb{R}^N, \tag{4.6b}$$

where, a_{T^0} and b_{T^0} denote, for any $T^0 \in \mathcal{T}_H^0$, suitable restrictions of the bilinear forms a and b, satisfying the properties

$$\sum_{T^0 \in \mathcal{T}_H^0} a_{T^0} = a \quad \text{and} \quad \sum_{T^0 \in \mathcal{T}_H^0} b_{T^0} = b.$$

Denoting by $n(T^1) := \#\{K^0 \in \mathcal{T}_H^0 \,:\, \partial K^0 \supset T^1\}$ the number of bulk elements sharing the interface element $T^1 \in \mathcal{T}_H^1$, such restrictions a_{T^0} and b_{T^0} can be defined as:

$$\begin{aligned} a_{T^0}(v,w) = (A^0\nabla^0 v^0, \nabla^0 w^0)_{T^0} &+ \sum_{T^1\subset\partial T^0} \frac{1}{n(T^1)}(A^1\nabla^1 v^1, \nabla^1 w^1)_{T^1} \\ &+ \sum_{T^1\subset\partial T^0} (B^1(v^0|_{T^0} - v^1), w^0|_{T^0} - w^1)_{T^1}, \end{aligned} \tag{4.7}$$

$$b_{T^0}(v,\mu) := \mu_{T^0} q_{T^0}(v) + \sum_{T^1\subset\partial T^0} \frac{1}{n(T^1)} \mu_{T^1} q_{T^1}(v). \tag{4.8}$$

In what follows, we establish the exponential decay of the operators $\mathcal{K}_{T^0}$ away from the element T^0. To quantify the decay, we introduce a notion of patches with respect to the coarse mesh $\mathcal{T}_H$. For an oversampling parameter $\ell \in \mathbb{N}$ and a union of elements $S^c \subset \mathcal{T}_H^c$ with $c \in \{0,1\}$, the ℓ-th order patch is defined recursively by

$$\mathsf{N}_\ell^c(S^c) := \mathsf{N}_1^c(\mathsf{N}_{\ell-1}^c(S^c)), \quad \ell \geq 2,$$

with $\mathsf{N}_1^c(S^c) := \mathsf{N}^c(S^c)$, as defined in (4.3). We also introduce a notation that jointly represents the bulk and interface components, namely $\mathsf{N}_\ell(S) := (\mathsf{N}_\ell^0(S^0), \mathsf{N}_\ell^1(S^1))$ for the ℓ-th order patches, and $\Omega \setminus \mathsf{N}_\ell(S) := (\Omega^0 \setminus \mathsf{N}_\ell^0(S^0), \Omega^1 \setminus \mathsf{N}_\ell^1(S^1))$ for their complement. Additionally, we abbreviate $\mathsf{N}_\ell(T^0) := \mathsf{N}_\ell(T^0, \partial T^0)$.

To formulate the desired exponential decay result, we require localized versions of the V-norm defined in (2.4). Instead of naively localizing it by merely restricting the H^1-norms on the bulk and interface domains to subdomains, we define, for tuples $S = (S^0, S^1)$ as above, the localized norm as follows:

$$\|\varphi\|_{V(S)}^2 := \|\nabla^0\varphi^0\|_{L^2(S^0)}^2 + \|\nabla^1\varphi^1\|_{L^2(S^1)}^2 + \sum_{\substack{\{T^1\subset\partial T^0\,:\\ T^0\subset S^0,\, T^1\subset S^1\}}} \|v^0|_{T^0} - v^1\|_{L^2(T^1)}^2. \tag{4.9}$$

This definition will prove more convenient for the subsequent proof. Note that the unrestricted version of this norm (i.e., the above definition with $S = (\Omega^0, \Omega^1)$), which we denote by $\|\cdot\|_{V(\Omega)}$, is equivalent to the energy norm, which, by Lemma 2.1, is in turn equivalent to the V-norm defined in (2.4) on the space V_0.

Theorem 4.1 (Exponential decay)**.** *There exists a constant $c > 0$ independent of H, ℓ, and T^0 such that for all $T^0 \in \mathcal{T}_H$ and $\ell \in \mathbb{N}$, it holds that*

$$\|\mathcal{K}_{T^0} v\|_{V(\Omega\setminus\mathsf{N}^\ell(T^0))} \lesssim \exp(-c\ell)\|\mathcal{K}_{T^0} v\|_{V(\Omega)}, \quad v \in V_0. \tag{4.10}$$

Proof. For a given $v \in V_0$, define $\varphi := \mathcal{K}_T v$. Introduce a cut-off function $\eta \in V_H^0$, defined on the bulk domain, and uniquely characterized by the following properties:

$$\begin{cases} \eta(x) = 0, & x \in \mathsf{N}_{\ell-1}^0(T^0), \\ \eta(x) = 1, & x \in \Omega^0 \setminus \mathsf{N}_\ell^0(T^0), \\ 0 \leq \eta(x) \leq 1, & x \in \mathsf{N}_\ell^0(T^0) \setminus \mathsf{N}_{\ell-1}^0(T^0). \end{cases} \tag{4.11}$$

By construction the cut-off function satisfies $\|\nabla^0\eta\|_{L^\infty} \lesssim H^{-1}$. Let the ring of elements containing the support of the gradient of η be denoted by

$$R_{T^0} = (R_{T^0}^0, R_{T^0}^1) := \mathsf{N}_\ell(T^0) \setminus \mathsf{N}_{\ell-1}(T^0). \tag{4.12}$$

In what follows, we assume that $\ell \geq 2$, which implies that $\overline{T^0} \cap \overline{R_{T^0}^0} = \emptyset$. For all elements $T^0 \in \mathcal{T}_H^0$ and $T^1 \in \mathcal{T}_H^1$ contained in the support of η, it thus holds that

$$\int_{T^0} \varphi^0 \,\mathrm{d}x = \int_{T^1} \varphi^1 \,\mathrm{d}\sigma = 0. \tag{4.13}$$

To prove this result, we use the identity $b(\varphi,\mu) = -b_{T^0}(v - \mathcal{I}_H v, \mu)$, which follows from (4.6b), together with the locality of the restricted bilinear form b_{T^0}.

Using definitions (2.6) and (4.9), the properties of η from (4.11), integration by parts, the coefficient bounds from (2.5), and (4.13), we obtain that

$$\begin{aligned}
&\|\varphi\|^2_{V(\Omega\setminus\mathsf{N}_\ell(T^0))}\\
&\quad\le (\eta A^0\nabla^0\varphi^0,\nabla^0\varphi^0)_{L^2(\Omega^0)}+(\eta A^1\nabla^1\varphi^1,\nabla^1\varphi^1)_{L^2(\Omega^1)}\\
&\qquad+\sum_{(i,j)\in E_0}(\eta B^1(\varphi^0_i-\varphi^1_j),\varphi^0_i-\varphi^1_j)_{L^2(\Omega^1_j)}\\
&\quad= a(\varphi,\eta\varphi)-(A^0\nabla^0\varphi^0,(\nabla^0\eta)\varphi^0)_{L^2(\Omega^0)}-(A^1\nabla^1\varphi^1,(\nabla^1\eta)\varphi^1)_{L^2(\Omega^1)}\\
&\quad\lesssim |b(\lambda,\eta\varphi)|+\|\nabla^0\varphi^0\|^2_{L^2(R^0_{T^0})}+\|\nabla^1\varphi^1\|^2_{L^2(R^1_{T^0})}.
\end{aligned}\tag{4.14}$$

In the last step, we have tested (4.6a) with $\eta\varphi$ and used that $a_{T^0}(\mathcal{I}_H v,\eta\varphi)=0$.

We estimate the first term on the right-hand side of (4.14) using the properties of η from (4.11), in combination with (4.13), yielding

$$\begin{aligned}
|b(\lambda,\eta\varphi)| &= \Big|\sum_{c\in\{0,1\}}\sum_{K^c\subset R^c_{T^0}}\lambda_{K^c}q_{K^c}(\eta\varphi)\Big|\\
&\lesssim \sum_{c\in\{0,1\}}\Big(H^{-d+c+2}\sum_{K^c\subset R^c_{T^0}}|\lambda_{K^c}|^2\Big)^{1/2}\|\nabla^c\varphi^c\|_{L^2(R^c_{T^0})}.
\end{aligned}\tag{4.15}$$

To derive bounds on the entries of the vector $\lambda\in\mathbb{R}^N$, we employ element and face bubble functions, as introduced for the proof of Lemma 3.1. By testing (4.6a) with $b_{K^0}=(v_{K^0},0)$ and using (3.7), we obtain, for any $K^0\subset R^0_{T^0}$, that

$$\begin{aligned}
|\lambda_{K^0}| &= |b(\lambda,b_{K^0})| = |a(\varphi,b_{K^0})| = |(A^0\nabla^0\varphi^0,\nabla^0 v_{K^0})_{L^2(\Omega^0)}\\
&\lesssim H^{d/2-1}\|\nabla^0\varphi^0\|_{L^2(K^0)}.
\end{aligned}$$

The second equality follows from the fact that $a_{T^0}(\mathcal{I}_H v,b_{K^0})=0$. Summing over all $K^0\subset R^0_{T^0}$ then yields

$$H^{-d+2}\sum_{K^0\subset R^0_{T^0}}|\lambda_{K^0}|^2\lesssim\|\nabla^0\varphi^0\|^2_{L^2(R^0_{T^0})}.\tag{4.16}$$

To derive a similar bound for the entries λ_{K^1} associated with $K^1\subset R^1_{T^0}$, we employ a trace inequality for φ^0 of the form

$$\|\varphi^0\|_{L^2(\partial T^0)}\lesssim H^{-\frac12}\|\varphi^0\|_{L^2(T^0)}+H^{\frac12}\|\nabla^0\varphi^0\|_{L^2(T^0)}\lesssim H^{\frac12}\|\nabla^0\varphi^0\|_{L^2(T^0)},\tag{4.17}$$

where the last estimate follows from the Poincaré inequality, which is applicable due to (4.13). Testing (4.6a) with $b_{K^1}=(0,v_{K^1})$, and using that $a_{T^0}(\mathcal{I}_H v,b_{K^1})=0$ together with stability estimate (3.7), we obtain, for any $K^1\subset R^1_{T^0}$, that

$$\begin{aligned}
|\lambda_{K^1}| &= |b(\lambda,b_{K^1})| = |a(\varphi,b_{K^1})|\\
&= |(A^1\nabla^1\varphi^1,\nabla^1 v_{K^1})_{L^2(K^1)}+\sum_{K^0\subset\omega_{K^1}}(B(\varphi^0|_{K^0}-\varphi^1),-v_{K^1})_{L^2(K^1)}|\\
&\lesssim H^{d/2}\|\nabla^0\varphi^0\|_{L^2(\omega_{K^1})}+H^{(d-1)/2-1}\|\nabla^1\varphi^1\|_{L^2(K^1)},
\end{aligned}$$

where ω_{K^1} denotes the union of the two bulk elements sharing the interface K^1. Summing over all $K^1\subset R^1_{T^0}$, we obtain that

$$\sum_{K^1\subset R^1_{T^0}}H^{-d+3}|\lambda_{K^1}|^2\lesssim\|\nabla^0\varphi^0\|^2_{L^2(\mathsf{N}^0(R^0_{T^0}))}+\|\nabla^1\varphi^1\|^2_{L^2(R^1_{T^0})}.\tag{4.18}$$

Combining (4.16) and (4.18), we obtain that

$$|b(\lambda,\eta\varphi)|\lesssim\|\nabla^0\varphi^0\|^2_{L^2(\mathsf{N}^0(R^0_{T^0}))}+\|\nabla^1\varphi^1\|^2_{L^2(R^1_{T^0})}.$$

We conclude that there exists a constant $C > 0$, independent of H, ℓ, and T^0, such that the following estimate holds for all $\ell \geq 2$:

$$\|\varphi\|^2_{V(\Omega\setminus\mathsf{N}_\ell(T^0))} \leq C\|\varphi\|^2_{V(\mathsf{N}^{\ell+1}(T^0)\setminus\mathsf{N}_{\ell-2}(T^0))}.$$

By the index shift $\ell \leftarrow \ell - 1$, we obtain, for all $\ell \geq 3$, that

$$\begin{aligned}\|\varphi\|^2_{V(\Omega\setminus\mathsf{N}_\ell(T^0))} &\leq \|\varphi\|^2_{V(\Omega\setminus\mathsf{N}_{\ell-1}(T^0))} \leq C\|\varphi\|^2_{V(\mathsf{N}_\ell(T^0))\setminus\mathsf{N}_{\ell-3}(T^0))} \\ &= C\left(\|\varphi\|^2_{V(\Omega\setminus\mathsf{N}_{\ell-3}(T^0))} - \|\varphi\|^2_{V(\Omega\setminus\mathsf{N}_\ell(T^0))}\right).\end{aligned}$$

Rearranging terms and defining $\gamma := \frac{C}{1+C} < 1$, we obtain the recursive inequality

$$\|\varphi\|^2_{V(\Omega\setminus\mathsf{N}^\ell(T^0))} \leq \gamma\|\varphi\|^2_{V(\Omega\setminus\mathsf{N}^{\ell-3}(T^0))} \leq \gamma^{\lfloor \ell/3 \rfloor}\|\varphi\|^2_{V(\Omega)},$$

and, noting that there exist constants $C, c > 0$ such that $\gamma^{\lfloor \ell/3 \rfloor/2} \leq C\exp(-c\ell)$, the assertion can be concluded for $\ell \geq 3$. For $\ell \in \{1, 2\}$, the result follows from a scaling argument (with a possible different hidden constant). □

5. Localization

The exponential decay properties established in the previous section motivate the localized computation of the prototypical LOD basis functions. The localization strategy proposed here, based on the approach presented in [HLM25], overcomes a key limitation of the naive localization method, which restricts problem (3.5) to the ℓ-th order patches. For this naive approach, the localization error deteriorates as the mesh is refined if the parameter ℓ remains fixed; see [MP14, Mai21].

To formalize the localization strategy, we introduce the localized spaces

$$V^\ell_{T^0} := \{v \in V_0 \,:\, \mathrm{supp}(v) \subset \mathsf{N}_\ell(T^0)\}, \tag{5.1}$$

$$M^\ell_{T^0} := \left\{\mu \in \mathbb{R}^N \,:\, \mu_{T^c} = 0 \text{ for all } T^c \subset \Omega^c \setminus \mathsf{N}^c_\ell(T^0),\ c \in \{0,1\}\right\}. \tag{5.2}$$

Localized element correctors can then be defined for any $v \in V_0$ as the unique

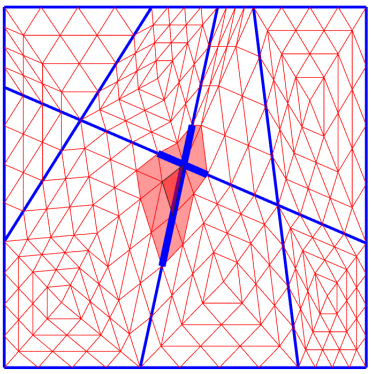

Figure 5.1. Example of a first-order patch $\mathsf{N}_1(T^0)$, around a coarse bulk element. The shaded red area marks the bulk elements of the patch whereas the opaque red marks the element T. The thickened blue lines mark the interface elements belonging to the patch.

solution $(\mathcal{K}^\ell_{T^0}v, \lambda^\ell) \in V^\ell_{T^0} \times M^\ell_{T^0}$ satisfying

$$a(\mathcal{K}^\ell_{T^0}v, w) + b(w, \lambda^\ell) = a_{T^0}(\mathcal{I}_H v, w), \qquad \text{for all } w \in V^\ell_{T^0}, \tag{5.3a}$$

$$b(\mathcal{K}^\ell_{T^0}v, \mu) = -\,b_{T^0}(v - \mathcal{I}_H v, \mu), \qquad \text{for all } \mu \in M^\ell_{T^0}. \tag{5.3b}$$

We define a localized version of the operator $\mathcal{R}$ as:

$$\mathcal{R}^\ell v := (\mathcal{I}_H - \mathcal{K}^\ell)v, \qquad \mathcal{K}^\ell v := \sum_{T^0 \in \mathcal{T}_H^0} \mathcal{K}^\ell_{T^0} v. \tag{5.4}$$

In what follows, we show that $\mathcal{R}^\ell$ provides an exponentially accurate (quasi-)local approximation of $\mathcal{R}$. The proof relies on a localized version of the decay result stated in Theorem 4.1, which is formulated in the following corollary.

Corollary 5.1 (Local version of exponential decay)**.** *For all $T^0 \in \mathcal{T}_H$ and all $m, \ell \in \mathbb{N}$, it holds that*

$$\|\mathcal{K}^\ell_{T^0} v\|_{V(\Omega \setminus \mathsf{N}^m(T^0))} \lesssim \exp(-cm) \|\mathcal{K}^\ell_{T^0} v\|_{V(\mathsf{N}^\ell(T^0))}, \quad v \in V^0,$$

where c is the constant from Theorem 4.1.

Proof. We apply Theorem 4.1 with $\mathcal{K}_{T^0}$, V, and $\mathsf{N}^\ell(T^0)$ replaced by $\mathcal{K}^\ell_{T^0}$, $V^\ell_{T^0}$, and $\mathsf{N}^m(T^0)$, respectively. The proof carries over without modification. □

We now proceed to the exponential approximation result.

Theorem 5.2 (Localization error)**.** *For all $\ell \in \mathbb{N}$, it holds that*

$$\|(\mathcal{R} - \mathcal{R}^\ell)v\|_V \lesssim \ell^{(d-1)/2} \exp(-c\ell) \|v\|_V, \quad v \in V_0, \tag{5.5}$$

where c is the constant from Theorem 4.1.

Proof. Let $e := (\mathcal{R} - \mathcal{R}^\ell)v$ denote the localization error. Using the coercivity of the bilinear form a from Lemma 2.1, the fact that $a(\tilde{V}_H, w) = 0$, and the definition of $\mathcal{R}^\ell$ from (5.4), we obtain the following representation of the localization error:

$$\|e\|_V^2 \lesssim a(e,e) = -a(\mathcal{R}^\ell v, e) = -a(\mathcal{I}_H v, e) + \sum_{T^0 \in \mathcal{T}_H^0} a(\mathcal{K}^\ell_{T^0} v, e). \tag{5.6}$$

We now analyze each term in the sum on the right-hand side individually. Recalling the definition of the cut-off function from (4.11) and testing (5.3a) with the test function $(1-\eta)e \in V^\ell_{T^0}$, we obtain that

$$\begin{aligned} a(\mathcal{K}^\ell_{T^0} v, e) &= a(\mathcal{K}^\ell_{T^0} v, (1-\eta)e + \eta e) \\ &= -b((1-\eta)e, \lambda^\ell) + a_{T^0}(\mathcal{I}_H v, (1-\eta)e) + a(\mathcal{K}^\ell_{T^0} v, \eta e) \\ &=: \Xi_1 + \Xi_2 + \Xi_3. \end{aligned}$$

To estimate the term Ξ_1, we employ arguments analogous to those used in (4.15), replacing η with $1-\eta$ and φ with e. Note that, not only φ, but also e satisfies the vanishing mean condition (4.13), which leads to the following estimate:

$$\begin{aligned} |\Xi_1| &= \Big| \sum_{c \in \{0,1\}} \sum_{K^c \subset R^c_{T^0}} \lambda^\ell_{K^c} q_{K^c}((1-\eta)e) \Big| \\ &\lesssim \sum_{c \in \{0,1\}} \Big(H^{-d+c+2} \sum_{K^c \subset R^c_{T^0}} |\lambda^\ell_{K^c}|^2 \Big)^{1/2} \|\nabla^c e^c\|_{L^2(R^c_{T^0})}, \end{aligned}$$

where $R^c_{T^0}$ is defined as in (4.12). To estimate the entries of $\lambda^\ell \in M^\ell_{T^0}$, we follow the same steps as in the proof of Theorem 4.1, specifically (4.16) and (4.18), yielding

$$\sum_{c \in \{0,1\}} H^{-d+c+2} \sum_{K^c \subset R^c_{T^0}} |\lambda^\ell_{T^c}|^2 \lesssim \|\mathcal{K}^\ell_{T^0} v\|^2_{V(\mathsf{N}(R_{T^0}))}. \tag{5.7}$$

Inserting this into the above estimate for $|\Xi_1|$ gives

$$|\Xi_1| \lesssim \|\mathcal{K}^\ell_{T^0} v\|_{V(\mathsf{N}(R_{T^0}))} \|e\|_{V(R_{T^0})}.$$

Next, we consider the term Ξ_2. Noting that $a_{T^0}(\mathcal{I}_H v, (1-\eta)e) = a_{T^0}(\mathcal{I}_H v, e)$, it follows that, upon summing over all bulk elements $T^0 \in \mathcal{T}_H^0$, the term Ξ_2 cancels exactly with the term $-a(\mathcal{I}_H v, e)$ on the right-hand side of (5.6).

To estimate Ξ_3, we use that the intersection of the supports of the functions $\mathcal{K}_{T^0}^\ell v$ and ηe is contained in R_{T^0}, which yields that

$$\Xi_3 \lesssim |a(\mathcal{K}_{T^0}^\ell v, \eta e)| \lesssim \|\mathcal{K}_{T^0}^\ell v\|_{V(R_{T^0})} \|\eta e\|_{V(R_{T^0})} \lesssim \|\mathcal{K}_{T^0}^\ell v\|_{V(R_{T^0})} \|e\|_{V(\mathsf{N}(R_{T^0}))},$$

where in the last step we employed definition (4.9), the trace inequality (4.17), and the fact that e satisfies (4.13).

Combining the estimates for the terms Ξ_1, Ξ_2, and Ξ_3, and applying Corollary 5.1, along with the finite overlap of the sets $\{\mathsf{N}(R_{T^0}) : T^0 \in \mathcal{T}_H^0\}$, we obtain

$$\begin{aligned}
\|e\|_V^2 &\lesssim \sum_{T^0 \in \mathcal{T}_H^0} \|\mathcal{K}_{T^0}^\ell v\|_{V(\mathsf{N}(R_{T^0}))} \|e\|_{V(\mathsf{N}(R_{T^0}))} \\
&\lesssim \exp(-c\ell) \sum_{T^0 \in \mathcal{T}_H^0} \|\mathcal{K}_{T^0}^\ell v\|_V \|e\|_{V(\mathsf{N}(R_{T^0}))} \\
&\lesssim \exp(-c\ell) \sqrt{\sum_{T^0 \in \mathcal{T}_H^0} \|\mathcal{K}_{T^0}^\ell v\|_V^2} \sqrt{\sum_{T^0 \in \mathcal{T}_H^0} \|e\|_{V(\mathsf{N}(R_{T^0}))}^2} \\
&\lesssim \ell^{(d-1)/2} \exp(-c\ell) \sqrt{\sum_{T^0 \in \mathcal{T}_H^0} \|\mathcal{K}_{T^0}^\ell v\|_V^2} \|e\|_V. \qquad (5.8)
\end{aligned}$$

It remains to estimate the term $\|\mathcal{K}_{T^0}^\ell v\|_V$. To this end, we test (5.3a) with the function $\mathcal{K}_{T^0}^\ell v$ and apply the identity obtained by testing (5.3b) with λ^ℓ. Using Lemma 2.1, this yields the following estimate:

$$\|\mathcal{K}_{T^0}^\ell v\|_V^2 \lesssim a(\mathcal{K}_{T^0}^\ell v, \mathcal{K}_{T^0}^\ell v) = -a_{T^0}(\mathcal{I}_H v, \mathcal{K}_{T^0}^\ell v) - b_{T^0}(v - \mathcal{I}_H v, \lambda^\ell). \qquad (5.9)$$

We bound the first term on the right-hand side of the latter estimate as

$$|a_{T^0}(\mathcal{I}_H v, \mathcal{K}_{T^0}^\ell v)| \lesssim \|\mathcal{I}_H v\|_{V(T^0)} \|\mathcal{K}_{T^0}^\ell v\|_{V(T^0)} \lesssim \|v\|_{V(\mathsf{N}(T^0))} \|\mathcal{K}_{T^0}^\ell v\|_{V(T^0)},$$

where we have used (4.1) and the trace inequality, cf. (4.17). Above $\|\cdot\|_{V(T^0)}$ is used as an abbreviation for $\|\cdot\|_{V(T^0,\partial T^0)}$.

For the second term, we obtain the estimate

$$\begin{aligned}
&|b_{T^0}(v - \mathcal{I}_H v, \lambda^\ell)| \\
&\quad \lesssim H^{-d/2+1} |\lambda_{T^0}^\ell| \|\nabla^0 v^0\|_{L^2(T^0)} + \Big(H^{-d+3} \sum_{T^1 \subset \partial T^0} |\lambda_{T^1}^\ell|^2\Big)^{1/2} \|\nabla^1 v^1\|_{L^2(\partial T^0)} \\
&\quad \lesssim \|\mathcal{K}_{T^0}^\ell v\|_{V(\mathsf{N}(T^0))} \|v\|_{V(\mathsf{N}(T^0))},
\end{aligned}$$

where we used arguments similar to those in the proof of (5.7) to estimate the components of λ^ℓ. Inserting the two preceding estimates into (5.9) yields

$$\|\mathcal{K}_{T^0}^\ell v\|_{V(\mathsf{N}_\ell(T^0))}^2 \lesssim \|v\|_{V(\mathsf{N}_\ell(T^0))} \|\mathcal{K}_{T^0}^\ell v\|_{V(\mathsf{N}_\ell(T^0))},$$

and, in turn, inserting this estimate into (5.8) yields the assertion. □

6. Practical multiscale method

In this section, we introduce a practical multiscale method based on locally computable basis functions. This is justified by the exponential decay of the globally defined prototypical basis functions. We define the localized basis functions as

$$\tilde{\varphi}_{T^c}^\ell := \mathcal{R}^\ell b_{T^c}, \qquad (6.1)$$

and define the localized multiscale space as their span:

$$\tilde{V}_H^\ell := \operatorname{span}\{\tilde{\varphi}_{T^c}^\ell : T^c \in \mathcal{T}_H^c,\, c \in \{0,1\}\}.$$

We emphasize that the operator $\mathcal{R}^\ell$ depends on its argument only through its QOI, as introduced in (3.1). Consequently, the definition (6.1) of $\tilde{\varphi}^\ell_{T^c}$ is independent of the specific choice of bubble functions, provided the Kronecker-delta condition (3.6) on the QOI is satisfied. Note that, for a bulk element $T^0 \in \mathcal{T}^0_H$, computing the associated basis function $\tilde{\varphi}^\ell_{T^0}$ requires solving local problems of the form (5.3) for all bulk elements in the first-order patch surrounding T^0. Similarly, for an interface element $T^1 \in \mathcal{T}^1_H$, the basis function $\tilde{\varphi}^\ell_{T^1}$ is obtained by solving local problems of the form (5.3) for each bulk element that shares the face T^1. Figure 6.1 shows examples of a bulk basis function $\tilde{\varphi}^\ell_{T^0}$ and an interface basis function $\tilde{\varphi}^\ell_{T^1}$ for $\ell = 4$.

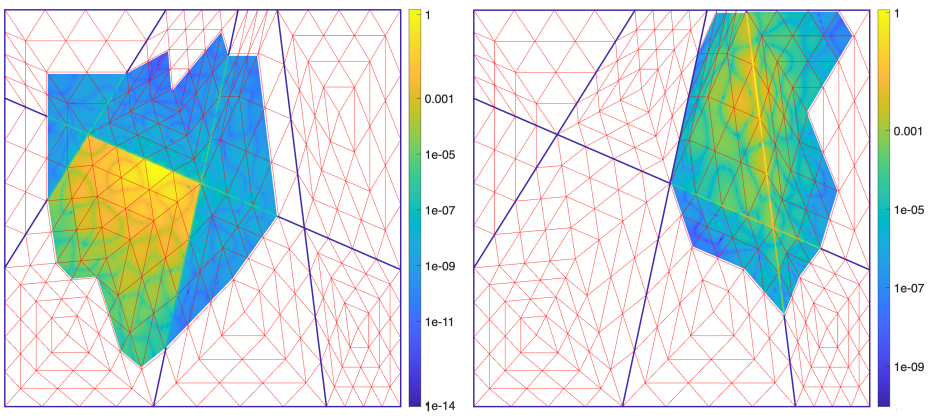

(a) (b)

FIGURE 6.1. Examples of basis functions corresponding to a coarse mesh bulk element (a) and a coarse mesh interface element (b) using a patch spreading $\ell = 4$ layers.

The LOD method seeks the unique function $\tilde{u}^\ell_H \in \tilde{V}^\ell_H$ such that

$$a(\tilde{u}^\ell_H, \tilde{v}^\ell_H) = F(\tilde{v}^\ell_H), \quad \text{for all } \tilde{v}^\ell_H \in \tilde{V}^\ell_H. \tag{6.2}$$

The following theorem provides a convergence result for the LOD approximation.

Theorem 6.1 (Localized method)**.** *The localized multiscale method* (6.2) *is well-posed, and, for any right-hand side F of the form* (2.7)*, with components $f^0 \in H^s(\Omega^0)$ and $f^1 \in H^s(\Omega^1)$, where $s \in \{0, 1\}$, the following error estimate holds:*

$$\|u - \tilde{u}^\ell_H\|_V \lesssim H^{1+s}|f|_s + \ell^{(d-1)/2}\exp(-c\ell)|f|_0, \tag{6.3}$$

where the (semi-)norm $|\cdot|_s$ is defined in (3.12)*.*

Proof. After establishing Theorem 3.2 and Theorem 5.2 the proof follows the arguments of [MP20, Thm. 5.2] closely. We omit the details for the sake of brevity. □

We emphasize that, for a practical computation of the LOD basis functions defined in (6.1), the problems (5.3), which are local but infinite-dimensional, still need to be solved. In practice, we approximate the solutions to these problems using a (local) fine-scale discretization. For codimensions $c \in \{0, 1\}$, let $\mathcal{T}^c_h$ denote a mesh obtained by uniform refinement of the coarse mesh $\mathcal{T}^c_H$. The fine mesh size $h < H$ should be chosen such that $\mathcal{T}^c_h$ resolves the fine-scale oscillations of the coefficients of the problem at hand. Throughout the derivation of the method, we replace the space V_0 by its finite-dimensional subspace $V_{0,h}$, consisting of continuous, piecewise

linear functions defined with respect to $\mathcal{T}_h^c$. Specifically, for problem (5.3), this means posing it on a finite-dimensional version of $V_{T^0}^\ell$ as defined in (5.1), but with V_0 replaced by $V_{0,h}$. In the fully discrete convergence analysis, V_0 is likewise replaced by $V_{0,h}$, and most arguments carry over directly; see, e.g., [MP20, Ch. 4.4], for a discussion of technical details that also arise in the present setting. This yields an a priori error estimate for the fully discrete LOD approximation similar to Theorem 6.1, but with respect to the fine-scale finite element solution in $V_{0,h}$. An estimate with respect to the weak solution of the original PDE then follows from the triangle inequality combined with standard finite element approximation results; see, e.g., [HMM23b, Thm. 2] for the present mixed-dimensional setting.

7. Generalization to complex-shaped coarse elements

The assumption made in Section 3 and used throughout, namely that the coarse meshes $\mathcal{T}_H^c$, $c \in \{0,1\}$, are simplicial or quadrilateral/hexahedral, can be relaxed. A closer inspection reveals that the construction of the method and its error analysis relies only on the ability to:

(1) construct bubble functions satisfying the Kronecker–delta property (3.6) and the inverse inequality (3.7);
(2) construct a suitable partition of unity on the meshes $\mathcal{T}_H^c$, $c \in \{0,1\}$, for defining a quasi-interpolation operator in place of definition (4.1);
(3) establish local Poincaré-type inequalities used to prove that properties (4.2) hold for the resulting partition-of-unity-based quasi-interpolation.

Such assumptions also hold in a more general setting for shape-regular and quasi-uniform coarse meshes $\mathcal{T}_H^c$, $c \in \{0,1\}$, consisting of simply connected elements formed as unions of fine mesh elements from $\mathcal{T}_h^c$. See Figure 7.1 for an example of such a mesh. For these meshes, quasi-uniformity and non-degeneracy can be characterized as follows: for each element $T^c \in \mathcal{T}_H^c$, with $c \in \{0,1\}$, there exist inscribed and circumscribed balls $B_R^c(x_0) \subset T^c \subset B_{R'}^c(x_0)$ such that

$$\rho_0 H \leq R \leq R' \leq \rho_1 H,$$

where $\rho_0, \rho_1 > 0$ are moderate constants.

Item 1 holds in the above general setting since a bubble function can be constructed as $v_{T^c}(x) = \alpha \max(0, R - |x - x_0|)$ with support on T^c. By choosing the constant α appropriately, this function satisfies the Kronecker–delta property (3.6). Clearly, also the inverse inequality (3.7) is satisfied.

To construct a partition of unity suitable for defining a quasi-interpolation operator replacing (4.1), as required in Item 2, we first introduce open covers of Ω^c for $c \in \{0,1\}$. The subdomains in these covers correspond to elements $T^c \in \mathcal{T}_H^c$ and are defined as the first-order element patches with respect to $\mathcal{T}_H^c$, i.e., $U_{T^c} = \mathsf{N}^c(T^c)$ with patches defined as in (4.3). Define the functions

$$\tilde{\Lambda}_{T^c}(x) = \begin{cases} \mathrm{dist}^c(x, \partial U_{T^c}), & x \in U_{T^c}, \\ 0, & \text{otherwise}, \end{cases}$$

where $\mathrm{dist}^c(x, \partial U_{T^c})$ denotes the intrinsic distance from x to the boundary ∂U_{T^c}, considering only paths contained entirely in Ω^c. Using these functions, the partition of unity for $c \in \{0,1\}$ consists of functions Λ_{T^c} defined for each $T^c \in \mathcal{T}_H^c$ by

$$\Lambda_{T^c}(x) = \frac{\tilde{\Lambda}_{T^c}(x)}{\sum_{S^c \in \mathcal{T}_H^c} \tilde{\Lambda}_{S^c}(x)}. \tag{7.1}$$

Since the coarse meshes are assumed to be quasi-uniform and shape-regular, the supports of the partition of unity functions overlap sufficiently to guarantee that the denominator in (7.1) remains uniformly positive. Moreover, it follows that

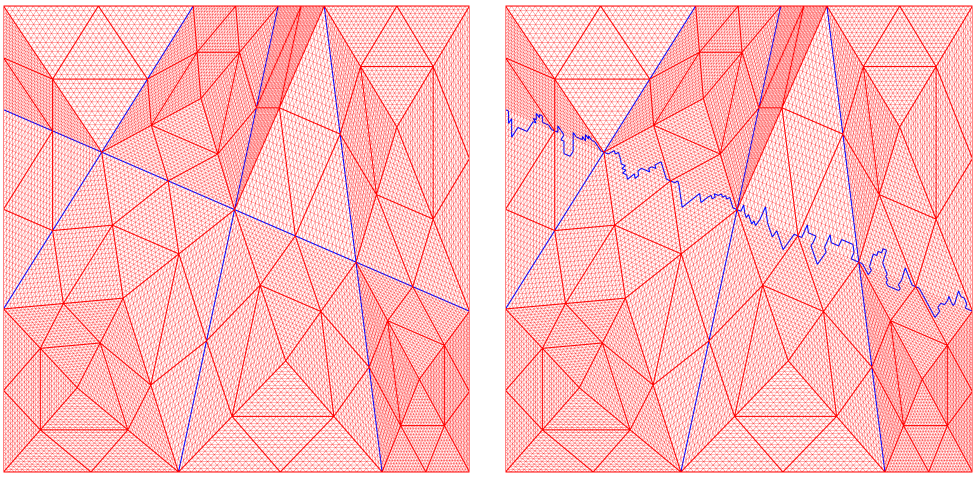

(a) (b)

FIGURE 7.1. A domain with straight interfaces (blue lines) and simplicial coarse mesh elements (red thick lines) is shown in (a). A modified domain with an interface that follows the fine mesh (red thin lines) and leads to non-convex, complex-shaped coarse mesh elements is shown in (b).

each Λ_{T^c} is Lipschitz continuous, with a Lipschitz constant proportional to H^{-1}. A quasi-interpolation operator can then be constructed as

$$\mathcal{I}_H^c v^c := \sum_{T^c \in \mathcal{T}_H^c} q_{T^c}(v^c)\Lambda_{T^c};$$

see [Car99] for the analysis of such operators, and also [HMM23a].

Finally, concerning Item 3, we assume that each element $T^c \in \mathcal{T}_H^c$ satisfies a local Poincaré inequality on its first-order patch:

$$\|v - q_{\mathsf{N}^c(T^c)}(v)\|_{L^2(\mathsf{N}^c(T^c))} \leq CH\|\nabla^c v\|_{L^2(\mathsf{N}^c(T^c))}, \tag{7.2}$$

for all $v \in H^1(\mathsf{N}^c(T^c))$, where $q_{\mathsf{N}^c(T^c)}$ is defined as in (3.1) but with $\mathsf{N}^c(T^c)$ in place of T^c. According to [Rui12], for an inequality of the form (7.2) to hold, three conditions are required: a uniform bound on the size of $\mathsf{N}^c(T^c)$; the existence, for each $\mathsf{N}^c(T^c)$, of a fixed finite cone C such that every boundary point of $\mathsf{N}^c(T^c)$ is the vertex of a cone C_x, congruent to C and contained in $\mathsf{N}^c(T^c)$; and a constant $\delta_0 > 0$ such that for all $\delta \in (0, \delta_0)$, the inner set

$$\mathsf{N}_\delta^c(T^c) := \{x \in \mathsf{N}^c(T^c) \,:\, \mathrm{dist}^c(x, \partial\mathsf{N}^c(T^c)) > \delta\}$$

is connected. These assumptions exclude domains with narrow regions but are not very restrictive in our context, as our elements are constructed as unions of connected fine-scale elements.

8. Numerical experiments

In this section, we present a numerical investigation of the proposed multiscale method. The first two numerical examples examine the convergence of the energy norm of the error, $\|u_h - \tilde{u}_H^\ell\|_a$, with respect to the coarse mesh size H for the localized method defined in (6.2). Here, u_h denotes the solution obtained from the fitted finite element method on the mesh $\mathcal{T}_h$, as introduced in [HMM23b]. The first example considers a problem with smoothly varying coefficients, while the second addresses rapidly oscillating coefficients A^0 and A^1. The third example investigates

the localization error of the method, measured in the energy norm, with respect to the oversampling parameter ℓ, for a coarse mesh containing complex-shaped elements. In this case, a simplified variant of method (6.2) is employed. Throughout this section, H and h denote the coarse and fine mesh sizes, respectively.

We consider the domain $\Omega = (0,1)^2$ with four interfaces, as illustrated in Figure 8.1. The convergence with respect to the coarse mesh size H is studied for $H \in \{1, \frac{1}{2}, \frac{1}{4}, \frac{1}{8}, \frac{1}{16}\}$. The corresponding coarse meshes are generated by successive uniform refinement of an initial coarse mesh $\mathcal{T}_H$ with $H = 1$, capturing the geometry. The mesh $\mathcal{T}_h$, with mesh size $h = 1/64$, is obtained by uniform refinement of the finest coarse mesh corresponding to $H = \frac{1}{16}$. Figure 8.1 shows the coarse mesh for $H = \frac{1}{4}$, along with a zoomed-in view of the underlying fine mesh. Note that the mesh sizes H and h have to be understood relative to the subdomain size.

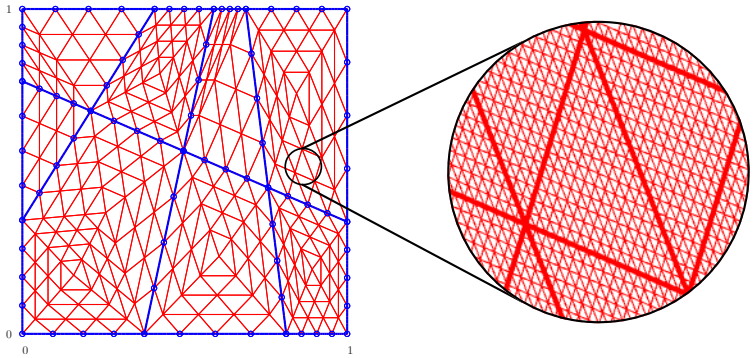

FIGURE 8.1. The domain Ω used for the numerical experiments. Here, the blue lines are the interfaces Ω^1 and the coarse mesh corresponding to $H = \frac{1}{4}$ is shown in red. The fine scale mesh is shown in the zoomed-in part.

In the first numerical experiment, we solve the problem (2.8) on Ω with data $A^0 = 1$, $A^1 = 1$, $B^1 = 1$, $f^0 = \sin(\pi x)\sin(\pi y)$, and $f^1 = x + 2y$, and plot the resulting errors for fixed oversampling parameters ℓ, as a function of the coarse mesh size H. Figure 8.2(a) shows the finite element reference solution, while (b) shows the convergence behavior of the proposed method. The error is measured in the energy norm relative to the finite element reference solution. We observe that, for fixed ℓ, the error first decreases with optimal order $\mathcal{O}(H^2)$. Beyond a certain point, the localization error becomes dominant, and the convergence curve reaches a plateau. The level of this plateau decreases with increasing oversampling parameter ℓ. This behavior is consistent with the theoretical result in Theorem 6.1. Importantly, for fixed ℓ, the error does not increase again after reaching the plateau, an undesirable effect observed, for example, in [MP14, Mai21]. These improved stability properties of the proposed method can be attributed to the refined localization procedure introduced in Section 5.

In the second numerical example, we consider coefficients A^0 and A^1 that vary rapidly on the fine scale. The coefficient A^0 is chosen to be piecewise constant on the fine mesh $\mathcal{T}_h$, taking random values in the range $[0.01, 1]$, while A^1 is defined as $A^1 = \sin(30\pi x)\sin(30\pi y) + 2$. For this example, again we let $B^1 = 1$, $f^0 = \sin(\pi x)\sin(\pi y)$, and $f^1 = x + 2y$. Figure 8.3(a) shows the corresponding finite element solution, and (b) presents the resulting convergence behavior. The observed convergence is qualitatively similar to that of the previous numerical example.

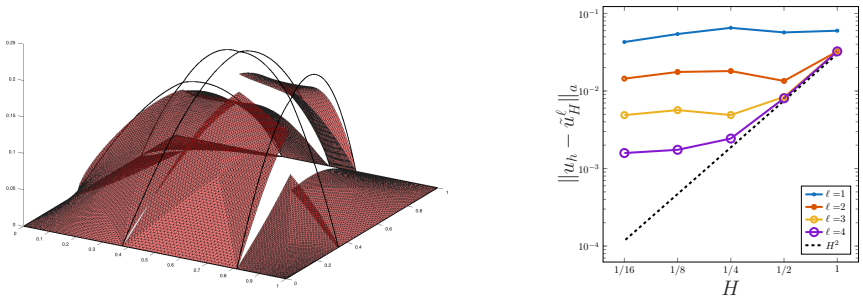

(a) (b)

FIGURE 8.2. In (a), the solution to the problem defined by $A^0 = 1$, $A^1 = 1$, $B^1 = 1$, $f^0 = \sin(\pi x)\sin(\pi y)$, and $f^1 = x+2y$ is shown. In (b), we see the convergence results, the energy norm of the error between the reference solution u_h and approximations $\tilde{u}_H^\ell$ with respect to H is shown for different oversampling parameters ℓ.

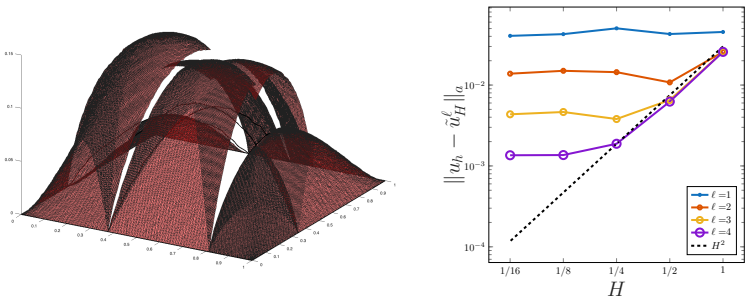

(a) (b)

FIGURE 8.3. In (a), the solution of the problem with random, piecewise constant A^0 on the fine mesh, with random values in the range $[0.01,\ 1]$. Here, $A^1 = \sin(30\pi x)\sin(30\pi y) + 2$, $B^1 = 1$, $f^0 = \sin(\pi x)\sin(\pi y)$, and $f^1 = x + 2y$. In (b), the convergence of said problem with regards to the coarse mesh size H, for different oversampling parameters ℓ is shown.

In the final numerical example, we consider a generalized coarse mesh consisting of complex-shaped elements; see Section 7. The domain and corresponding coarse mesh are shown in Figure 7.1(b). In this experiment, A^0 is again chosen to be piecewise constant on the fine mesh $\mathcal{T}_h$, with random values in the range $[0.01, 1]$, while $A^1 = 1$, $B^1 = 1$, $f^0 = 1$, and $f^1 = 1$. The construction of the method for these complex-shaped coarse meshes follows the procedure described in Section 7. For implementation purposes, we deviate from the stabilized localization strategy presented in Section 5 and instead employ a simplified localization approach, where the global problems (3.5) defining the basis functions are localized directly. Note that this method is affected by the previously described deterioration of errors if the oversampling parameter is not increased logarithmically as the mesh size decreases. The resulting solution and convergence behavior for $h = \frac{1}{32}$ and $H = \frac{1}{2}$, with respect to the oversampling parameter ℓ, are shown in Figure 8.4. We emphasize that for this choice of f^0 and f^1, the first term on the right-hand side of

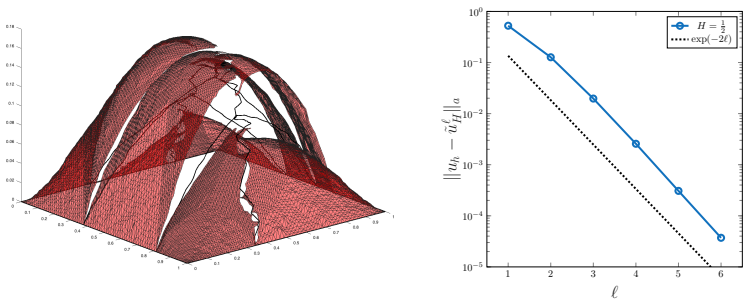

(a) (b)

FIGURE 8.4. In (a), the finite element solution of the problem with complex-shaped coarse mesh is shown, and in (b) is the convergence of said problem based on the number of layers the patches spread. Here, A^0 is a piecewise constant, random coefficient within $[0.01, 1]$, $A^1 = 1$, $B^1 = 1$, $f^0 = 1$ and $f^1 = 1$. We have $h = \frac{1}{32}$ and $H = \frac{1}{2}$.

error estimate (6.3) vanishes and only the exponentially decaying localization error remains. The observed decay behavior is again consistent with Theorem 3.2.

ACKNOWLEDGMENTS

M. Hauck acknowledges funding from the Deutsche Forschungsgemeinschaft (DFG, German Research Foundation) – Project-ID 258734477 – SFB 1173. Furthermore, A. Målqvist acknowledges funding from the Swedish Research Council (VR) – Project-ID 2023-03258_VR.

REFERENCES

[AGPR19] A. Arrarás, F. J. Gaspar, L. Portero, and C. Rodrigo. Mixed-dimensional geometric multigrid methods for single-phase flow in fractured porous media. *SIAM J. Sci. Comput.*, 41(5):B1082–B1114, 2019.

[AHP21] R. Altmann, P. Henning, and D. Peterseim. Numerical homogenization beyond scale separation. *Acta Numer.*, 30:1–86, 2021.

[BCH+14] E. Burman, S. Claus, P. Hansbo, M. G. Larson, and A. Massing. CutFEM: Discretizing geometry and partial differential equations. *Int. J. Numer. Methods Eng.*, 104(7):472–501, 2014.

[BCO94] I. Babuška, G. Caloz, and J. E. Osborn. Special finite element methods for a class of second order elliptic problems with rough coefficients. *SIAM J. Numer. Anal.*, 31(4):945–981, 1994.

[BHL+18] E. Burman, P. Hansbo, M. G. Larson, K. Larsson, and A. Massing. Finite element approximation of the Laplace–Beltrami operator on a surface with boundary. *Numer. Math.*, 141(1):141–172, 2018.

[BL11] I. Babuška and R. Lipton. Optimal local approximation spaces for generalized finite element methods with application to multiscale problems. *Multiscale Model. Simul.*, 9(1):373–406, 2011.

[BNY18] W. M. Boon, J. M. Nordbotten, and I. Yotov. Robust discretization of flow in fractured porous media. *SIAM J. Numer. Anal.*, 56(4):2203–2233, 2018.

[BO83] I. Babuška and J. E. Osborn. Generalized finite element methods: their performance and their relation to mixed methods. *SIAM J. Numer. Anal.*, 20(3):510–536, 1983.

[Car99] C. Carstensen. Quasi-interpolation and a posteriori error analysis in finite element methods. *ESAIM Math. Model. Numer. Anal. (M2AN)*, 33(6):1187–1202, 1999.

[DE13] G. Dziuk and C. M. Elliott. Finite element methods for surface pdes. *Acta Numer.*, 22:289–396, 2013.

[DHM23] Z. Dong, M. Hauck, and R. Maier. An improved high-order method for elliptic multiscale problems. *SIAM J. Numer. Anal.*, 61(4):1918–1937, 2023.

[DPFS17] M. Del Pra, A. Fumagalli, and A. Scotti. Well posedness of fully coupled fracture/bulk darcy flow with xfem. *SIAM J. Numer. Anal.*, 55(2):785–811, 2017.

[Dzi88] G. Dziuk. *Finite Elements for the Beltrami operator on arbitrary surfaces*, page 142–155. Springer Berlin Heidelberg, 1988.

[EE03] W. E and B. Engquist. The heterogeneous multiscale methods. *Commun. Math. Sci.*, 1(1):87–132, 2003.

[EE05] W. E and B. Engquist. The heterogeneous multi-scale method for homogenization problems. In *Multiscale methods in science and engineering*, volume 44 of *Lect. Notes Comput. Sci. Eng.*, pages 89–110. Springer, Berlin, Heidelberg, 2005.

[EG17] A. Ern and J.-L. Guermond. Finite element quasi-interpolation and best approximation. *ESAIM Math. Model. Numer. Anal.*, 51(4):1367–1385, 2017.

[ER12] C. M. Elliott and T. Ranner. Finite element analysis for a coupled bulk-surface partial differential equation. *IMA J. Numer. Anal.*, 33(2):377–402, 2012.

[FHKP24] P. Freese, M. Hauck, T. Keil, and D. Peterseim. A super-localized generalized finite element method. *Numer. Math.*, 156(1):205–235, 2024.

[FK18] A. Fumagalli and E. Keilegavlen. Dual virtual element method for discrete fractures networks. *SIAM J. Sci. Comput.*, 40(1):B228–B258, 2018.

[FKO+22] M. Fritz, T. Köppl, J. T. Oden, A. Wagner, B. Wohlmuth, and C. Wu. A 1D–0D–3D coupled model for simulating blood flow and transport processes in breast tissue. *Int. J. Numer. Methods Biomed. Eng.*, 38(7), 2022.

[HLM25] M. Hauck, A. Lozinski, and R. Maier. A generalized framework for higher-order localized orthogonal decomposition methods. *arXiv e-print*, 2025.

[HMM23a] M. Hauck, R. Maier, and A. Målqvist. An algebraic multiscale method for spatial network models. ArXiv e-print 2312.09752, 2023.

[HMM23b] F. Hellman, A. Målqvist, and M. Mosquera. Well-posedness and finite element approximation of mixed dimensional partial differential equations. *BIT Numer. Math.*, 64(1), 2023.

[HMW21] F. Hellman, A. Målqvist, and S. Wang. Numerical upscaling for heterogeneous materials in fractured domains. *ESAIM: Math. Model. Numer. Anal.*, 55, 2021.

[HP13] P. Henning and D. Peterseim. Oversampling for the multiscale finite element method. *Multiscale Model. Simul.*, 11(4):1149–1175, 2013.

[HP22] M. Hauck and D. Peterseim. Multi-resolution localized orthogonal decomposition for Helmholtz problems. *Multiscale Model. Simul.*,

20(2):657–684, 2022.

[HP23] M. Hauck and D. Peterseim. Super-localization of elliptic multiscale problems. *Math. Comp.*, 92(341):981–1003, 2023.

[Mai21] R. Maier. A high-order approach to elliptic multiscale problems with general unstructured coefficients. *SIAM J. Numer. Anal.*, 59(2):1067–1089, 2021.

[MJR05] V. Martin, J. Jaffré, and J. E. Roberts. Modeling fractures and barriers as interfaces for flow in porous media. *SIAM J. Sci. Comput.*, 26(5):1667–1691, 2005.

[MP14] A. Målqvist and D. Peterseim. Localization of elliptic multiscale problems. *Math. Comp.*, 83(290):2583–2603, 2014.

[MP20] A. Målqvist and D. Peterseim. *Numerical homogenization by localized orthogonal decomposition*, volume 5 of *SIAM Spotlights*. Society for Industrial and Applied Mathematics (SIAM), Philadelphia, PA, 2020.

[MSD22] C. Ma, R. Scheichl, and T. Dodwell. Novel design and analysis of generalized finite element methods based on locally optimal spectral approximations. *SIAM J. Numer. Anal.*, 60(1):244–273, 2022.

[ORG09] M. A. Olshanskii, A. Reusken, and J. Grande. A finite element method for elliptic equations on surfaces. *SIAM J. Numer. Anal.*, 47(5):3339–3358, 2009.

[OS19] H. Owhadi and C. Scovel. *Operator-adapted wavelets, fast solvers, and numerical homogenization*, volume 35 of *Cambridge Monographs on Applied and Computational Mathematics*. Cambridge University Press, Cambridge, 2019.

[Owh17] H. Owhadi. Multigrid with rough coefficients and multiresolution operator decomposition from hierarchical information games. *SIAM Rev.*, 59(1):99–149, 2017.

[Rui12] D. Ruiz. On the uniformity of the constant in the Poincaré inequality. *Adv. Nonlinear Stud.*, 12(4):889–903, 2012.

* Institute for Applied and Numerical Mathematics, Karlsruhe Institute of Technology, Englerstr. 2, 76131 Karlsruhe, Germany

Email address: moritz.hauck@kit.edu

† Department of Mathematical Sciences, Chalmers University of Technology and University of Gothenburg, Göteborg 412 96, Sweden

Email address: {axel,malinni}@chalmers.se